

Near-zero thermal expansion and phase transition in $\text{In}_{0.5}(\text{ZrMg})_{0.75}\text{Mo}_3\text{O}_{12}$

Luciana P. Prisco and Patricia I. Pontón

Departamento de Engenharia Química e de Materiais, Pontifícia Universidade Católica, 22451-900 Rio de Janeiro, RJ, Brasil

Waldeci Paraguassu

Faculdade de Física, Universidade Federal do Pará, Belém, PA 66075-110, Brasil

Carl P. Romao

Department of Chemistry, Dalhousie University, Halifax, Nova Scotia B3H 4R2, Canada

Mary Anne White

Department of Chemistry, Dalhousie University, Halifax, Nova Scotia B3H 4R2, Canada; Institute for Research in Materials, Dalhousie University, Halifax, Nova Scotia B3H 4R2, Canada; and Department of Physics and Atmospheric Science, Dalhousie University, Halifax, Nova Scotia B3H 4R2, Canada

Bojan A. Marinkovic^{a)}

Departamento de Engenharia Química e de Materiais, Pontifícia Universidade Católica, 22451-900 Rio de Janeiro, RJ, Brasil

(Received 9 March 2016; accepted 24 August 2016)

Physical properties of $\text{In}_{0.5}(\text{ZrMg})_{0.75}\text{Mo}_3\text{O}_{12}$, including the coefficient of thermal expansion, phase stability, hygroscopicity, and decomposition temperature have been thoroughly studied by *in situ* x-ray powder diffraction, Raman spectroscopy and thermal methods. These investigations show that $\text{In}_{0.5}(\text{ZrMg})_{0.75}\text{Mo}_3\text{O}_{12}$ exists in a monoclinic phase ($P2_1/a$) at room temperature and transforms to an orthorhombic ($Pbcn$) phase at ~ 82 °C. In the orthorhombic form this material presents intrinsic near-zero thermal expansion ($-0.16 \times 10^{-6} \text{ K}^{-1}$) in the range between 100 and 500 °C. The phase is not hygroscopic, but starts to decompose into its constituent oxides at temperatures higher than 700 °C. In comparison to the end member phase $\text{ZrMgMo}_3\text{O}_{12}$ in the $\text{In}_2\text{Mo}_3\text{O}_{12}$ – $\text{ZrMgMo}_3\text{O}_{12}$ solid solution, $\text{In}_{0.5}(\text{ZrMg})_{0.75}\text{Mo}_3\text{O}_{12}$ is less promising for near room-temperature applications due to the phase transition from monoclinic to orthorhombic slightly above room temperature. However, the orthorhombic phase of $\text{In}_{0.5}(\text{ZrMg})_{0.75}\text{Mo}_3\text{O}_{12}$ has potential for applications that require zero thermal expansion at temperatures higher than 100 °C.

I. INTRODUCTION

The orthorhombic space group $Pbcn$ (60) accommodates a large number of open-framework phases with the general chemical formula $\text{A}_2\text{M}_3\text{O}_{12}$.^{1–3} In this formula M is a hexavalent cation, such as Mo^{6+} or W^{6+} (although, P^{5+} has been reported⁴ as an element capable of partial substitution for W^{6+} or Mo^{6+}) forming 4-coordinated polyhedra, while A can be any small rare earth or some other trivalent cation from Al^{3+} to Y^{3+} , within an octahedral environment.^{5–8} Tetrahedra and octahedra build an open-framework crystal structure through connected vertices. Strain screening is made possible by the open-framework structure⁹ and solid solutions can be synthesized with almost any combination of these cations and, therefore, there is considerable chemical and physical

flexibility within the $\text{A}_2\text{M}_3\text{O}_{12}$ family. Trivalent cations occupy one independent general 8d site, while hexavalent cations occupy two independent crystallographic positions, one general 8d and one special 4c, and oxygens adopt six independent general 8d positions. This peculiar open framework, which is related to the garnet structure by removal of the 8-coordinated cations, is responsible for the striking physical properties of these phases, such as negative or near-zero coefficients of thermal expansion (CTE), and considerable ionic conductivity.^{10–14} If the trivalent cation is substituted by a 1:1 mixture of tetravalent (A: Hf or Zr) and divalent cations (B: Mg) a new family ($\text{ABM}_3\text{O}_{12}$) is formed, assuming a lower symmetry $Pna2_1$ (33) space group. The atomic structure of these compounds was recently resolved for orthorhombic $\text{ZrMgMo}_3\text{O}_{12}$ by Romao et al.,¹⁵ who established that tetravalent and divalent cations occupy distinct general 4a sites, while hexavalent cations and oxygen anions occupy three and twelve independent 4a sites, respectively. The physical properties of three $\text{ABM}_3\text{O}_{12}$ materials

Contributing Editor: Ian M. Reaney

^{a)}Address all correspondence to this author.

e-mail: bojan@puc-rio.br

DOI: 10.1557/jmr.2016.329

($\text{HfMgW}_3\text{O}_{12}$, $\text{HfMgMo}_3\text{O}_{12}$, and $\text{ZrMgMo}_3\text{O}_{12}$) have been reported, while solid solutions have been synthesized in the following systems: $\text{Al}_2\text{W}_3\text{O}_{12}$ – $\text{HfMgW}_3\text{O}_{12}$, $\text{Al}_2\text{W}_3\text{O}_{12}$ – $\text{ZrMgW}_3\text{O}_{12}$, $\text{In}_2\text{Mo}_3\text{O}_{12}$ – $\text{HfMgMo}_3\text{O}_{12}$, $\text{Fe}_2\text{Mo}_3\text{O}_{12}$ – $\text{ZrMgMo}_3\text{O}_{12}$, and $\text{Cr}_2\text{Mo}_3\text{O}_{12}$ – $\text{ZrMgMo}_3\text{O}_{12}$.^{16–23} The $\text{ABM}_3\text{O}_{12}$ compounds also have an open-framework crystal structure consisting of vertex-sharing coordination polyhedra. Therefore, near-zero or negative thermal expansion is expected, and has already been documented in the literature for some of these compounds (Table I). Note that orthorhombic $\text{A}_2\text{M}_3\text{O}_{12}$ and $\text{ABM}_3\text{O}_{12}$ phases can transform at lower temperatures to a denser structure with the monoclinic $P2_1/a$ (14) space group, which shows positive thermal expansion and, therefore, can be problematic for those applications where near-zero or negative thermal expansion is required. This phase transition is displacive²⁴ and can be characterized as primarily a static rotation of the coordination polyhedra. In some cases, hygroscopicity can occur due to the presence of nanochannels within the cation-deficient garnet structure. If these channels are sufficiently large as to admit water molecules, the water molecules will interact with the bridging oxygen anions and hinder their transverse vibrations and, therefore, prevent negative thermal expansion.

The thermal expansion, phase transitions, and hygroscopicity of $\text{In}_2\text{Mo}_3\text{O}_{12}$ – $\text{ZrMgMo}_3\text{O}_{12}$ solid solutions have not previously been reported, although these properties have been described for the end-members.^{15,25} As reported elsewhere²⁵ $\text{In}_2\text{Mo}_3\text{O}_{12}$ is monoclinic ($P2_1/a$) at room temperature and transforms to an orthorhombic ($Pbcn$) phase at a temperature of 335 °C; the latter presents a negative coefficient of thermal expansion ($-1.85 \times 10^{-6} \text{ K}^{-1}$) until at least 760 °C. The first report on $\text{ZrMgMo}_3\text{O}_{12}$ by Song et al.,²⁰ indicated that it exhibited an orthorhombic phase with a negative CTE ($-3.8 \times 10^{-6} \text{ K}^{-1}$) from –150 °C to 927 °C. However,

a more recent, thorough study,¹⁵ showed that $\text{ZrMgMo}_3\text{O}_{12}$ is in the orthorhombic phase between –126 °C and 700 °C with a very near-zero coefficient of thermal expansion ($0.16 \times 10^{-6} \text{ K}^{-1}$) from 25 °C to 450 °C, increasing by about an order of magnitude to $1.0 \times 10^{-6} \text{ K}^{-1}$ above 450 °C. Below –126 °C the orthorhombic phase transforms to monoclinic.

Therefore, the rule of mixtures predicts that a compound with the chemical formula $\text{In}_{2x}(\text{ZrMg})_{1-x}\text{Mo}_3\text{O}_{12}$, with $x = 0.25$ ($\text{In}:(\text{Zr} + \text{Mg}) = 1:3$) would present a negative CTE of about $-3.3 \times 10^{-6} \text{ K}^{-1}$ if the CTE determined by Song et al.,²⁰ were correct. The same approach predicts that the CTE of $\text{In}_{2x}(\text{ZrMg})_{1-x}\text{Mo}_3\text{O}_{12}$ ($x = 0.25$) should be an order of magnitude lower and, therefore, near zero ($-0.3 \times 10^{-6} \text{ K}^{-1}$), if the study carried out by Romao et al.¹⁵ gave a more accurate CTE of $\text{ZrMgMo}_3\text{O}_{12}$. It is, therefore, possible that $\text{In}_{0.5}(\text{ZrMg})_{0.75}\text{Mo}_3\text{O}_{12}$ could have a near-zero CTE over a large range of superambient temperatures. The phase transition temperature in this new material is also of concern since the addition of In, a more electronegative atom in comparison to Zr and Mg, would be expected to increase the temperature of the monoclinic (positive CTE) to orthorhombic (negative or near-zero CTE) phase transition. Also, the insertion of a larger cation (In^{3+}) into the crystal structure could potentially cause $\text{In}_{0.5}(\text{ZrMg})_{0.75}\text{Mo}_3\text{O}_{12}$ to become hygroscopic.

Therefore, it is scientifically and technologically relevant to study the thermal expansion, phase transition, and hygroscopicity of $\text{In}_{0.5}(\text{ZrMg})_{0.75}\text{Mo}_3\text{O}_{12}$; these three main properties are indispensable for the evaluation of the potential of such a material as a filler in composites or as a consolidated ceramic object. Also, the temperature at which the molybdate phase starts to decompose into constituent oxides, followed by MoO_3 sublimation, is relevant, considering the sintering processes necessary to produce dense polycrystalline objects.

TABLE I. Linear coefficients of thermal expansion (α) measured by XRPD and monoclinic–orthorhombic transition temperature for $\text{ABM}_3\text{O}_{12}$ compounds.

| Compound | $\alpha (10^{-6} \text{ K}^{-1})$ | Range (°C) | Transition temperature (°C) | References |
|---|-----------------------------------|-------------------|-----------------------------|------------|
| $\text{HfMgW}_3\text{O}_{12}$ | –1.2 –0.77 | 127–527 20–700 | 127–200 ... | 18 23 |
| $\text{Al}(\text{HfMg})_{0.5}\text{W}_3\text{O}_{12}$ | 1.32 | 20–700 | ... | 23 |
| $\text{HfMgMo}_3\text{O}_{12}$ | 1.02 | 25–740 | –98 | 10 |
| $\text{In}(\text{HfMg})_{0.5}\text{Mo}_3\text{O}_{12}$ | –0.4 0.16 | 225–650 25–450 | 152 –126 | 16 15 |
| $\text{ZrMgMo}_3\text{O}_{12}$ | 1.0 –3.3 | 450–700 27–727 | –126 <–150 | 15 20 |
| $\text{Cr}_{0.3}(\text{ZrMg})_{0.85}\text{Mo}_3\text{O}_{12}$ | 0.62 | 127–727 | <–170 | 21 |
| $\text{Cr}_{0.5}(\text{ZrMg})_{0.75}\text{Mo}_3\text{O}_{12}$ | 1.04 | 127–727 | ... | 21 |
| $\text{Al}_{0.2}(\text{ZrMg})_{0.9}\text{W}_3\text{O}_{12}$ | –0.058 | 130–650 | ... | 22 |
| $\text{Fe}_{0.2}(\text{ZrMg})_{0.9}\text{Mo}_3\text{O}_{12}$ | 1.64 | 27–727 | ... | 17 |
| $\text{Fe}_{0.4}(\text{ZrMg})_{0.8}\text{Mo}_3\text{O}_{12}$ | 2.02 | 27–727 | ... | 17 |

II. EXPERIMENTAL METHODS

A. Synthesis and consolidation of $\text{In}_{0.5}(\text{ZrMg})_{0.75}\text{Mo}_3\text{O}_{12}$

$\text{In}_{0.5}(\text{ZrMg})_{0.75}\text{Mo}_3\text{O}_{12}$ was synthesized through a total evaporation route from a stoichiometric mixture of 0.1 M aqueous solutions of $\text{Mg}(\text{NO}_3)_2$ (Sigma Aldrich, St. Louis, Missouri, 98%), $\text{In}(\text{NO}_3)_2$ (Sigma Aldrich, 99.9%), $(\text{NH}_4)_6\text{Mo}_7\text{O}_{24}\cdot 4\text{H}_2\text{O}$ (Isofar, 99%), and $\text{ZrO}(\text{NO}_3)_2$ (Johnson Matthey Company, New York, New York, 99.99%). Since 0.1 M aqueous solution of $\text{ZrO}(\text{NO}_3)_2$ is not soluble in water, it was necessary to add 100 mL of HNO_3 (Sigma Aldrich, 69%) until complete dissolution. The acidic solution obtained by the mixture of the four reagents ($\text{pH} = 0.35$) was continuously stirred and heated at 70 °C, until complete water evaporation (~ 12 h). Afterward, the as-prepared precursor material was oven dried at 100 °C for 8 h without any further post treatments. It was analyzed by differential scanning calorimetry (DSC) in a Perkin–Elmer (Seer Green, United Kingdom) Simultaneous Thermal Analyzer (STA-6000), using a heating rate of 5 K/min in air flux (20 mL/min), for determination of the crystallization temperature. The DSC curve (see Supplementary Materials) showed an exothermic peak at 718 °C, ascribed to the crystallization of $\text{In}_{0.5}(\text{ZrMg})_{0.75}\text{Mo}_3\text{O}_{12}$ from an amorphous precursor.

Therefore, the precursor powder was calcined at 750 °C (heating rate of 20 K/min) for 5 h in a Tubular Maitec–INTI FET 1600/H (Maitec, São Carlos, Brazil) furnace in air atmosphere, followed by an additional heating (with the same heating rate) to 800 °C with dwell time of 1 min.

Monolithic ceramics were prepared using the as-synthesized crystalline powder with the addition of 5 mass% of polyethylene glycol (98%; Vetec, Rio de Janeiro, Brazil) as binder, mixed with a small amount of distilled water until tacky and then pressed at 100 MPa of uniaxial pressure for 1 min. The as-prepared green cylindrical specimens were presintered at 800 °C for 1 h.

B. Characterization of $\text{In}_{0.5}(\text{ZrMg})_{0.75}\text{Mo}_3\text{O}_{12}$ powder

X-ray powder diffraction of the calcined powder was carried out in a D8 Discovery diffractometer (Bruker, Karlsruhe, Germany), using Cu K_α radiation in steps of 0.02° (1 s per step) from 10° to 80° (θ). In situ XRPD was carried out in a D8 Advance diffractometer using Cu K_α radiation, equipped with an XRK 900 reactor chamber (Anton Paar GmbH, Graz, Austria), at different temperatures (100, 200, 300, and 500 °C) in air atmosphere. The XRPD patterns were acquired in the range of 10°–80° (θ) with a step size of 0.02° (1 s per step). The analysis of raw data was performed using the Le Bail method with Topas 4.2 Software (Bruker) for determination of the intrinsic CTE and evaluation of the phase transition temperature.

DSC was carried out at a Perkin–Elmer Simultaneous Thermal Analyzer (STA 8000) in air flux (20 mL/min) in

the temperature range between –10 and 300 °C, at a heating rate of 10 K/min. The DSC was calibrated with In and Ag.

Thermogravimetry was performed in a Perkin–Elmer Simultaneous Thermal Analyzer (STA-6000) between 25 and 900 °C using a heating rate of 10 K/min in air flux (20 mL/min).

The morphology of the calcined powder was determined by a field-emission scanning electron microscope (FE-SEM) (JSM-6701F; JEOL Ltd., Tokyo, Japan) in secondary electron mode operating at 1 kV. The chemical composition was examined by energy-dispersive x-ray spectroscopy (EDS).

Raman spectroscopy was carried out in situ from room temperature to 250 °C using a Jobin Yvon T64000 spectrometer (Horiba Scientific, Longjumeau, France), which was equipped with a cooled charge-coupled device detector. The backscattering geometry was used to analyze the scattered light and the spectral excitation was provided by an Ar^+ laser using the 514.5 nm laser line. The slits were set for a spectral resolution of 2 cm^{-1} .

Additional Raman spectra of materials in the $\text{A}_2\text{M}_3\text{O}_{12}$ and $\text{ABM}_3\text{O}_{12}$ families (see Sec. III. B.) were acquired at room temperature using a Nicolet NXR 9650 FT-Raman spectrometer (Thermo Fisher Scientific, Waltham, Massachusetts) with a 1064 nm excitation laser, with spectral resolution of 1 cm^{-1} .

C. Characterization of $\text{In}_{0.5}(\text{ZrMg})_{0.75}\text{Mo}_3\text{O}_{12}$ monolithic ceramic

Relative density measurements of green and bulk specimens were carried out using Archimedes' principle. Wax was applied to the surface to prevent water entrance. Distilled water (30 °C, density 0.9957 g/cm³) was used as the liquid. The accuracy of the pellet mass measurement on the analytical balance was ± 0.001 g. As will be demonstrated in the Results section, crystalline $\text{In}_{0.5}(\text{ZrMg})_{0.75}\text{Mo}_3\text{O}_{12}$ powder was considered monophasic and monoclinic ($P2_1/a$) at room temperature for calculation of the theoretical density (3.44 g/cm³). The density of the green specimen was 62% of theoretical density (TD), while 80% of TD was determined for the pre-sintered samples.

Dilatometry of a bulk sample was performed in air using a NETZSCH dilatometer DIL 402C (NETZSCH Group, Selb, Germany) in the temperature range between 25 and 800 °C, with a heating rate of 10 K/min; the cooling rate was not controlled.

III. RESULTS AND DISCUSSION

A. Crystal system at room temperature and hygroscopicity of $\text{In}_{0.5}(\text{ZrMg})_{0.75}\text{Mo}_3\text{O}_{12}$

FE-SEM analysis [Fig. 1(a)] showed that the calcined powder was constituted of faceted sub-micron to

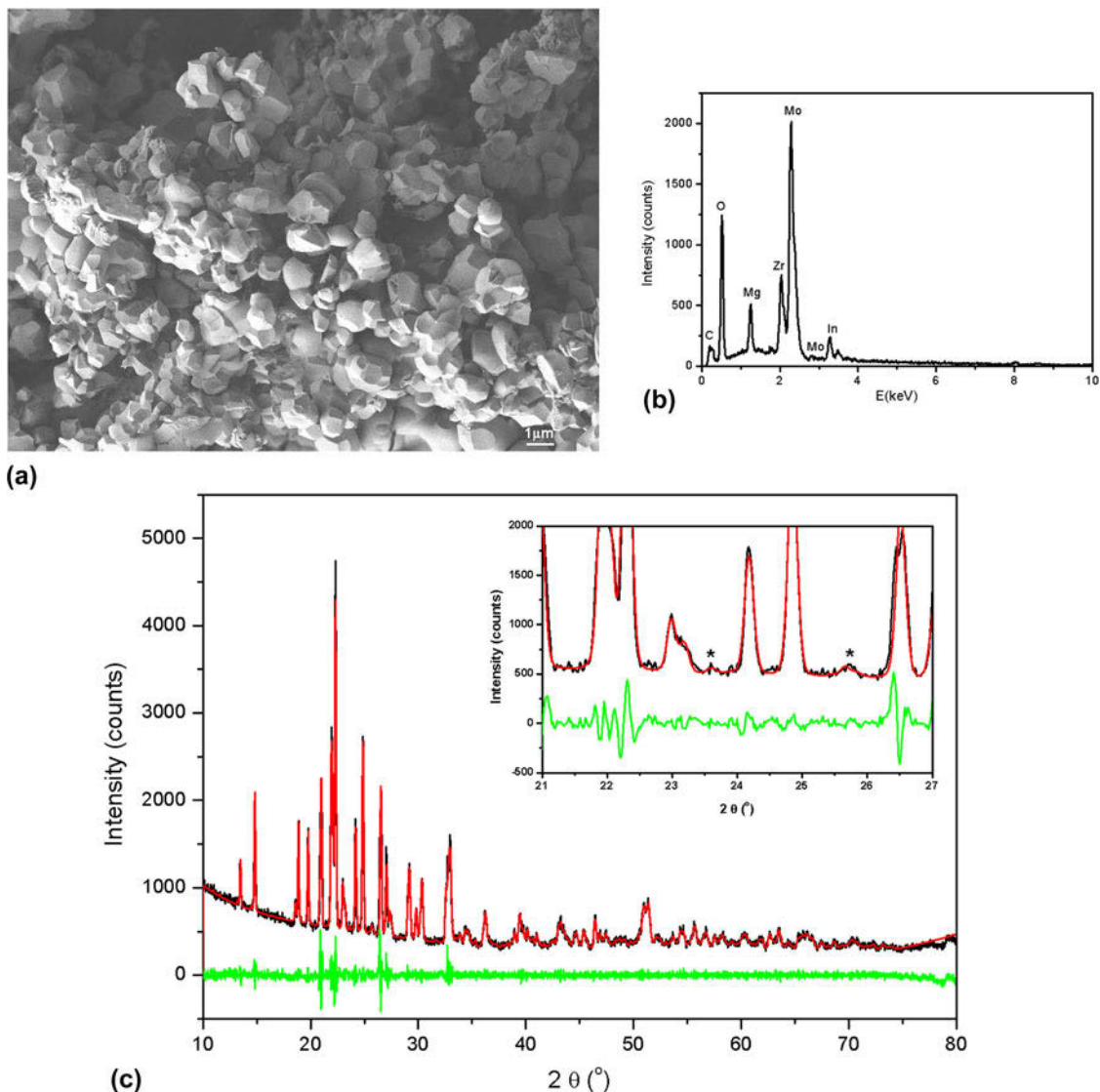


FIG. 1. (a) FEG-SEM image of $\text{In}_{0.5}(\text{ZrMg})_{0.75}\text{Mo}_3\text{O}_{12}$ powder, (b) EDS spectrum, and (c) room-temperature XRPD pattern, illustrating the Le Bail fit to the monoclinic $P2_1/a$ space group ($a = 16.2694 \text{ \AA}$, $b = 9.5610 \text{ \AA}$, $c = 18.9782 \text{ \AA}$ and $\beta = 125.56^\circ$); the experimental pattern is black, the calculated pattern is red and the difference plot is green [inset: magnified view of XRPD in the range between 21° and 27° (2θ), with two weak diffraction lines at 25.8° and 23.7° (2θ) related to the monoclinic system marked as *].

micron-sized particles, in the general range $0.7\text{--}1.6 \mu\text{m}$. EDS analysis [Fig. 1(b)] indicated that the stoichiometric ratio of the chemical elements is in agreement with the proposed formula $\text{In}_{0.5}(\text{ZrMg})_{0.75}\text{Mo}_3\text{O}_{12}$ (Table SI in Supplementary Material).

The room-temperature XRPD pattern [Fig. 1(c)] indicated that the calcined powder was monophasic and monoclinic ($P2_1/a$ space group), not orthorhombic. Two weak diffraction peaks at 25.8° and 23.7° (2θ), marked in the inset of Fig. 1(c), can be associated with a lower symmetry monoclinic space group ($P2_1/a$),¹⁰ and are absent in the orthorhombic space groups ($Pbcn$ and $Pna2_1$) adopted by members of the $\text{A}_2\text{M}_3\text{O}_{12}$ and $\text{ABM}_3\text{O}_{12}$ families. Therefore, the substitution of 1/4 of

the low electronegativity Zr (1.4) and Mg (1.2) atoms by In with higher electronegativity (1.7) significantly increases the thermal stability range of the monoclinic phase in comparison to the end-member compound $\text{ZrMgMo}_3\text{O}_{12}$ (transition temperature of -126°C).

Note that $\text{In}_{0.5}(\text{ZrMg})_{0.75}\text{Mo}_3\text{O}_{12}$ is not hygroscopic: its mass loss on heating to 600°C was negligible (<0.3 mass%) (Fig. 2). However, above 700°C significant mass loss occurs because of partial decomposition of $\text{In}_{0.5}(\text{ZrMg})_{0.75}\text{Mo}_3\text{O}_{12}$ into its constituent oxides followed by sublimation of MoO_3 .¹⁵ The absence of hygroscopicity is not unexpected since the end-members $\text{ZrMgMo}_3\text{O}_{12}$ and $\text{In}_2\text{Mo}_3\text{O}_{12}$ are not hygroscopic,¹⁵ and hygroscopicity in the $\text{A}_2\text{M}_3\text{O}_{12}$ family is generally

reported for the orthorhombic phases with large trivalent cations, such as rare earths from Y to Ho.²⁴ The evidence of partial molybdate decomposition above 700 °C (Fig. 2) might be an obstacle to attaining high densities during sintering.

B. Phase transition in $\text{In}_{0.5}(\text{ZrMg})_{0.75}\text{Mo}_3\text{O}_{12}$

The DSC thermogram of $\text{In}_{0.5}(\text{ZrMg})_{0.75}\text{Mo}_3\text{O}_{12}$ [Fig. 3(a)] shows an endothermic event on heating, associated with a monoclinic to orthorhombic phase transition, with an enthalpy change of 2.5 kJ/mol and an onset temperature of 82 °C. This kind of phase transition for the compounds belonging to the $\text{A}_2\text{M}_3\text{O}_{12}$ family is reported to be structurally subtle and comprises very low enthalpy changes ($\Delta H \leq 2$ kJ/mol),⁸ i.e., on the same order of magnitude as observed here for $\text{In}_{0.5}(\text{ZrMg})_{0.75}\text{Mo}_3\text{O}_{12}$. This is a displacive phase transition due to the breakage of secondary oxygen–oxygen bonds (the same ones responsible for the existence of molecular solid tetraoxides, such as RuO_4 and OsO_4) between neighboring polyhedra,^{1,26} resulting in more empty space within the orthorhombic crystal structure.

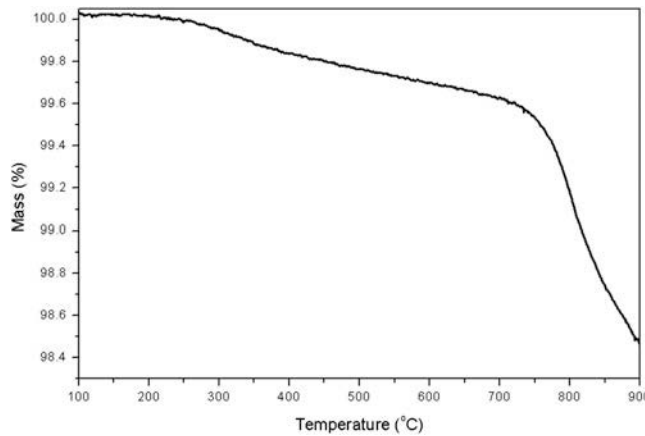


FIG. 2. TGA curve of $\text{In}_{0.5}(\text{ZrMg})_{0.75}\text{Mo}_3\text{O}_{12}$ powder.

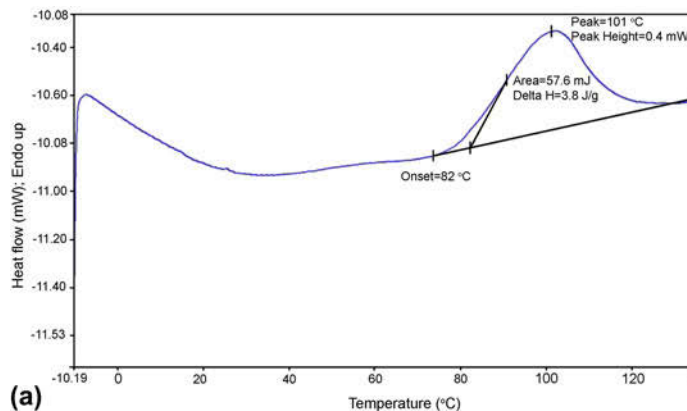
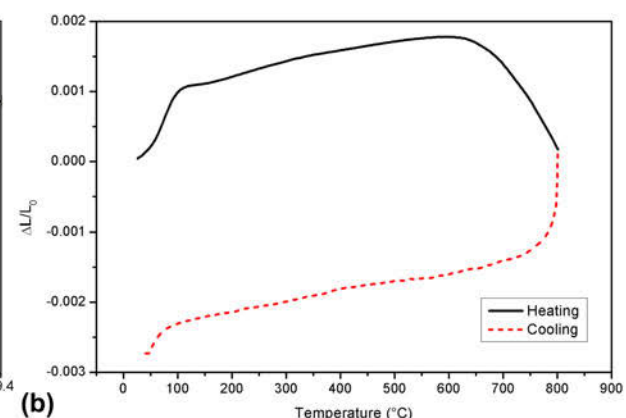


FIG. 3. (a) DSC curve of $\text{In}_{0.5}(\text{ZrMg})_{0.75}\text{Mo}_3\text{O}_{12}$ powder and (b) dilatometric curve of a pre-sintered specimen of $\text{In}_{0.5}(\text{ZrMg})_{0.75}\text{Mo}_3\text{O}_{12}$.

No primary bonds are broken during this event. Therefore, the phase transition is thermodynamically driven by the increase of vibrational entropy in the transition to a less dense structure (orthorhombic), causing more disorder (i.e., increase of distinctive configurations) in distribution of thermal energy over harmonic oscillators (atoms). The dilatometric curve of a pre-sintered specimen confirms this transition through an abrupt increase of sample length (thermal deformation) between 70 and 90 °C [Fig. 3(b)], characteristic of a phase transition from a dense to a more open crystal structure, such as in the case of the monoclinic ($P2_1/a$) to orthorhombic ($Pbcn$ or $Pna2_1$) transition, inherent to the $\text{A}_2\text{M}_3\text{O}_{12}$ and $\text{ABM}_3\text{O}_{12}$ families. This abrupt change of specimen length is not associated with water loss since the latter is insignificant for $\text{In}_{0.5}(\text{ZrMg})_{0.75}\text{Mo}_3\text{O}_{12}$.

In the $\text{A}_2\text{M}_3\text{O}_{12}$ family, the subtle structural differences that exist between $Pbcn$, $Pna2_1$, and $P2_1/a$ phases can be difficult to resolve by x-ray diffraction alone.^{15,18} Raman spectroscopy provides an important complementary technique because it is sensitive to different structural features. Specifically, there exist stretching modes of the AO_6 and MO_4 coordination polyhedra that are sensitive to the identity of the A and M cations.²⁷ Unlike the low-energy bending and librational modes, which involve coordinated motions of atoms throughout the unit cell, the energies of the stretching modes show significant differences for the $Pbcn$, $Pna2_1$, and $P2_1/a$ phases.^{15,27} However, the number of Raman-active vibrational modes in $\text{A}_2\text{M}_3\text{O}_{12}$ materials is large due to their large unit cells and the absence of atoms at special positions.^{15,27} Therefore, to quantify differences in the vibrational spectra between phases, a deconvolution approach has been used, using Fityk software.²⁸ This approach fits the spectra to peaks that represent bands rather than individual vibrations, an approach which is supported by previous computational and Raman studies.^{15,27,29–33}

In Fig. 4 the fitted stretching regions of the Raman spectra of $\text{In}_{0.5}(\text{ZrMg})_{0.75}\text{Mo}_3\text{O}_{12}$ at 40 and 250 °C are



shown. The fits were performed with pseudo-Voigt profile functions, with the goal of finding the minimum number of peaks required for a satisfactory fit. The criterion used was to deem the fit satisfactory when the addition of a new peak resulted in a reduction in the residual which was larger than the residual resulting from the error in fitting the shape of the largest stretching peak. Eight peaks were needed to fit the spectrum acquired at 40 °C [Fig. 4(a)], whereas the spectrum acquired at 250 °C [Fig. 4(b)] required only five peaks, indicating an increase in symmetry upon heating. This result is consistent with previous reports of transitions between monoclinic and orthorhombic phases in the $\text{A}_2\text{M}_3\text{O}_{12}$ family.^{29,32,33} However, peak deconvolution has not previously been applied to these materials. Therefore, we have additionally determined and deconvoluted the room-temperature Raman spectra of $\text{A}_2\text{M}_3\text{O}_{12}$ and $\text{ABM}_3\text{O}_{12}$ materials such as $\text{In}_2\text{Mo}_3\text{O}_{12}$, $\text{Al}_2\text{Mo}_3\text{O}_{12}$, $\text{ZrMgMo}_3\text{O}_{12}$, and $\text{Sc}_2\text{W}_3\text{O}_{12}$; all these phases synthesized as described elsewhere,²⁵ are known and were used here to make comparisons with $\text{In}_{0.5}(\text{ZrMg})_{0.75}\text{Mo}_3\text{O}_{12}$.

Figure 5 shows the stretching regions of the Raman spectra of $\text{In}_2\text{Mo}_3\text{O}_{12}$ and $\text{Al}_2\text{Mo}_3\text{O}_{12}$, two $\text{A}_2\text{M}_3\text{O}_{12}$

materials that adopt a monoclinic $P2_1/a$ phase at room temperature.^{25,34} In both cases, the deconvolution procedure revealed eight peaks. The significant differences in the positions and intensities of the peaks between the two materials can be attributed to the Al^{3+} cation participating in the stretches to a greater extent than Sc^{3+} due to the greater rigidity of the AlO_6 polyhedron.^{15,27} The identification of eight peaks in the spectra shown in Fig. 5 corroborates the $P2_1/a$ phase at room temperature for $\text{In}_{0.5}(\text{ZrMg})_{0.75}\text{Mo}_3\text{O}_{12}$.

In Fig. 6, the stretching regions of the Raman spectra of $\text{ZrMgMo}_3\text{O}_{12}$ and $\text{Sc}_2\text{W}_3\text{O}_{12}$, two materials whose orthorhombic phases are stable at room temperature,^{15,35} are shown. $\text{Sc}_2\text{W}_3\text{O}_{12}$ adopts a $Pbcn$ structure typical for $\text{A}_2\text{M}_3\text{O}_{12}$ materials,³⁵ whereas the related $Pna2_1$ phase of $\text{ZrMgMo}_3\text{O}_{12}$ has ordered Zr^{4+} and Mg^{2+} cations.¹⁵ $\text{A}'_{2x}(\text{A''Mg})_{1-x}\text{M}_3\text{O}_{12}$ materials such as $\text{In}_{0.5}(\text{ZrMg})_{0.75}\text{Mo}_3\text{O}_{12}$ can adopt $Pna2_1$ phases where the $\text{A''}(\text{Zr or Hf})$ and Mg atoms are ordered and the A' atom is disordered,²³ or $Pbcn$ phases where all three A site atoms are disordered.²³ Deconvolution of the stretching regions of the Raman spectra revealed 11 peaks for $\text{ZrMgMo}_3\text{O}_{12}$ and five for $\text{Sc}_2\text{W}_3\text{O}_{12}$. The large differences between the two can be attributed to the decrease in

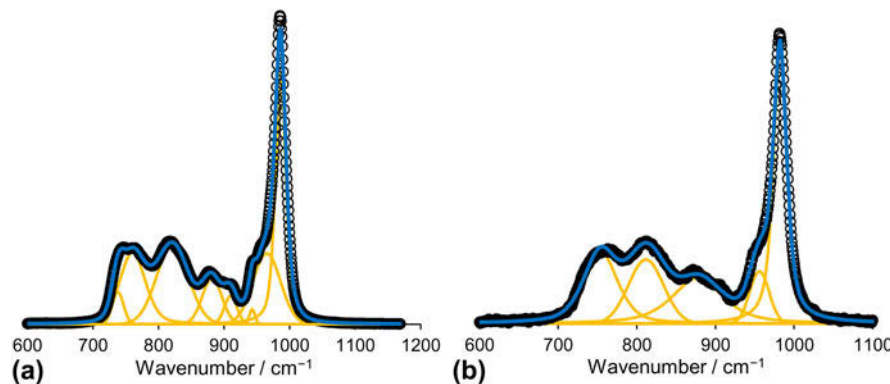


FIG. 4. Stretching regions of the Raman spectra of $\text{In}_{0.5}(\text{ZrMg})_{0.75}\text{Mo}_3\text{O}_{12}$ at (a) 40 °C and (b) 250 °C, showing experimental data (black circles), the fit to the data (blue line), and the peaks composing the fit (orange lines).

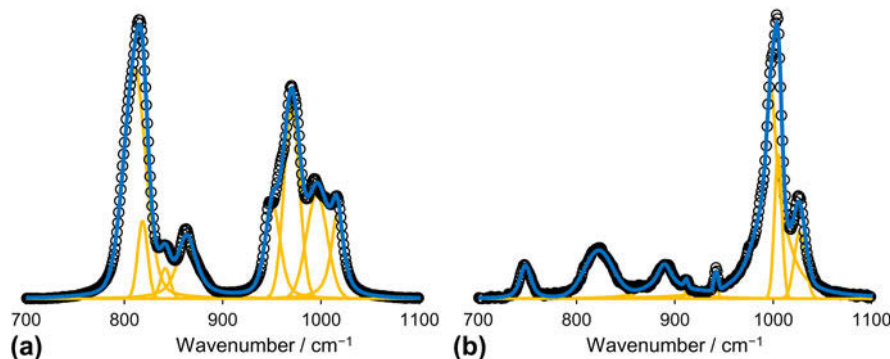


FIG. 5. Stretching regions of the Raman spectra of (a) $\text{In}_2\text{Mo}_3\text{O}_{12}$ and (b) $\text{Al}_2\text{Mo}_3\text{O}_{12}$ at room temperature, showing experimental data (black circles), the fit to the data (blue line), and the peaks composing the fit (orange lines). Both materials are in the $P2_1/a$ phase at this temperature.^{25,34}

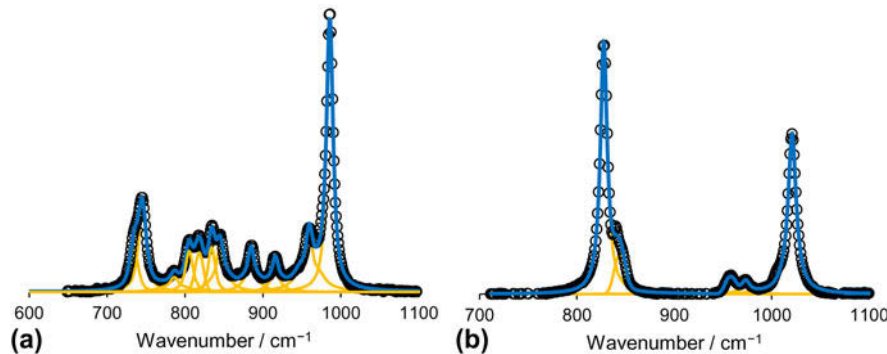


FIG. 6. Stretching regions of the Raman spectra of (a) $\text{ZrMgMo}_3\text{O}_{12}$ and (b) $\text{Sc}_2\text{W}_3\text{O}_{12}$ at room temperature, showing experimental data (black circles), the fit to the data (blue line), and the peaks composing the fit (orange lines). $\text{ZrMgMo}_3\text{O}_{12}$ is in the $Pna2_1$ phase while $\text{Sc}_2\text{W}_3\text{O}_{12}$ is in the $Pbcn$ phase at this temperature.^{15,35}

symmetry between $Pbcn$ and $Pna2_1$, and the differences in chemical bonding between the ZrO_6 and MgO_6 polyhedra.¹⁵ The presence of five peaks in the stretching region of the Raman spectrum of $\text{In}_{0.5}(\text{ZrMg})_{0.75}\text{Mo}_3\text{O}_{12}$ at 250 °C therefore corroborates its assignment to the $Pbcn$ phase, while the presence of eight peaks in the room temperature spectrum confirms the assignment of this phase to the monoclinic $P2_1/a$ space group as previously ascribed through XRPD [Fig. 1(a)]. The increased breadth of the peaks in Fig. 4 can be attributed to disorder at the A site.

C. Thermal expansion of orthorhombic $\text{In}_{0.5}(\text{ZrMg})_{0.75}\text{Mo}_3\text{O}_{12}$

Suzuki and Omote²³ showed for $\text{Al}_{2x}(\text{HfMg})_{1-x}\text{W}_3\text{O}_{12}$ that when x increases from 0 to ~ 0.3 , the space group changes to $Pbcn$ from a lower symmetry orthorhombic space group (originally thought to be $Pnma$ but now known to be $Pna2_1$).¹⁵ This agrees with our analysis of the Raman spectra of $\text{In}_{0.5}(\text{ZrMg})_{0.75}\text{Mo}_3\text{O}_{12}$ ($x = 0.25$), which attributed the spectrum at 250 °C, i.e., above the phase transition temperature, to the orthorhombic space group $Pbcn$ [see Supplementary Materials for all Raman spectra of $\text{In}_{0.5}(\text{ZrMg})_{0.75}\text{Mo}_3\text{O}_{12}$ from room temperature to 250 °C]. In situ XRPD (Fig. 7) additionally corroborates that the high temperature phase adopts the $Pbcn$ space group due to the absence of two closely spaced diffraction lines at around 13.5° (20), present in the case of $Pna2_1$ space group in accordance to the findings of Suzuki and Omote.²³ Figure 8 presents the dependence of the natural logarithm of unit-cell volume of $\text{In}_{0.5}(\text{ZrMg})_{0.75}\text{Mo}_3\text{O}_{12}$ in the orthorhombic ($Pbcn$) phase with temperature. The intrinsic linear CTE, calculated from the slope of this curve, gives a value very close to zero ($-0.16 \pm 0.07 \times 10^{-6} \text{ K}^{-1}$) between 100 and 500 °C, in reasonable agreement to the value estimated by the rule of mixtures ($-0.3 \times 10^{-6} \text{ K}^{-1}$), using the CTE of the end-member $\text{ZrMgMo}_3\text{O}_{12}$ reported by Romao et al.¹⁵ The CTE of $\text{In}_{0.5}(\text{ZrMg})_{0.75}\text{Mo}_3\text{O}_{12}$ is

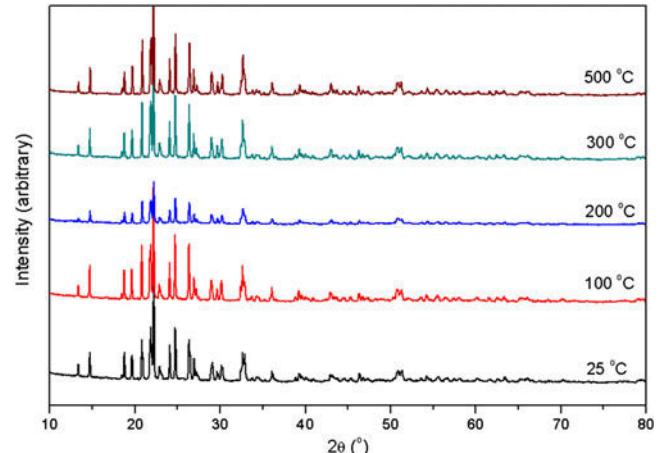


FIG. 7. In situ XRPD patterns of $\text{In}_{0.5}(\text{ZrMg})_{0.75}\text{Mo}_3\text{O}_{12}$ powder in the temperature range between 25 and 500 °C.

in the same range as $\text{ZrMgMo}_3\text{O}_{12}$ ($0.16 \times 10^{-6} \text{ K}^{-1}$), which is considered a near-zero thermal expansion material with a CTE similar to that of fused quartz and Invar.

It is worth noting that $\text{In}_{0.5}(\text{ZrMg})_{0.75}\text{Mo}_3\text{O}_{12}$ shows anisotropic expansion along its three crystallographic axes, as the a -axis expands and b - and c -axes contract on heating (Supplementary Material, Fig. S3). Thermal expansion anisotropy can be quantitatively expressed as the maximum difference between the axial thermal expansion coefficients ($\Delta\alpha_{\max}$) as proposed by Srikanth³⁶ and it was determined here to be $\Delta\alpha_{\max} = 9.2 \times 10^{-6} \text{ K}^{-1}$ (from 100 to 500 °C). This value is almost the same as previously determined for $\text{In}(\text{HfMg})_{0.5}\text{Mo}_3\text{O}_{12}$ ¹⁶ and is significantly lower than the values generally estimated for the phases from $\text{A}_2\text{M}_3\text{O}_{12}$ and $AB\text{M}_3\text{O}_{12}$ families.¹⁶ The CTE can also be obtained from the dilatometric curve, however, pronounced hysteresis [Fig. 3(b)] indicates microcrack healing within bulk specimens. Thus, the bulk CTE ($1.5 \times 10^{-6} \text{ K}^{-1}$) determined dilatometrically on heating from 100 to 500 °C is biased due to the microcracking contribution

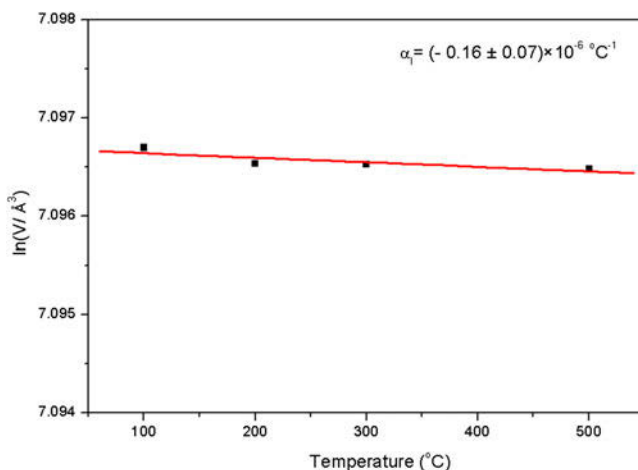


FIG. 8. Natural logarithm of the unit-cell volume of orthorhombic ($Pbcn$ space group) $\text{In}_{0.5}(\text{ZrMg})_{0.75}\text{Mo}_3\text{O}_{12}$ as a function of temperature.

increasing the CTE compared with the intrinsic CTE, a phenomenon previously documented that can occur on heating and cooling of bulk specimens.³⁷ It is possible that sintered bodies of $\text{In}_{0.5}(\text{ZrMg})_{0.75}\text{Mo}_3\text{O}_{12}$ with nanometric grains could exhibit a bulk CTE close to the intrinsic value due to reduction of microcracks in accordance with Griffith theory.³⁸

IV. CONCLUSIONS

$\text{In}_{0.5}(\text{ZrMg})_{0.75}\text{Mo}_3\text{O}_{12}$ is a novel non-hygroscopic and near-zero thermal expansion phase from the $\text{A}'_{2x}(\text{A}''\text{Mg})_{1-x}\text{M}_3\text{O}_{12}$ family. Nevertheless, distinct from the closer solid solution end-member, $\text{ZrMgMo}_3\text{O}_{12}$, it is monoclinic ($P2_1/a$) at room temperature and transforms to an orthorhombic ($Pbcn$) crystal system at ~ 82 °C. Above this temperature to 500 °C the orthorhombic phase shows a CTE of $(-0.16 \pm 0.07) \times 10^{-6} \text{ K}^{-1}$ and, therefore, is considered a near-zero thermal expansion material. At the temperatures higher than 700 °C this phase starts to decompose into its constituent oxides accompanied by MoO_3 volatilization. Therefore, special precautions should be used during sintering of this phase to achieve high densities and protect $\text{In}_{0.5}(\text{ZrMg})_{0.75}\text{Mo}_3\text{O}_{12}$ from decomposition. In comparison to the end-member phase $\text{ZrMgMo}_3\text{O}_{12}$ of the $\text{In}_2\text{Mo}_3\text{O}_{12}$ – $\text{ZrMgMo}_3\text{O}_{12}$ solid solution series, $\text{In}_{0.5}(\text{ZrMg})_{0.75}\text{Mo}_3\text{O}_{12}$ is generally less promising for application purposes due to the phase transition from monoclinic to orthorhombic crystal system slightly above room temperature. Nevertheless, $\text{In}_{0.5}(\text{ZrMg})_{0.75}\text{Mo}_3\text{O}_{12}$ is more isotropic in its thermal expansion along the three principal axes than generally reported for the phases from $\text{A}_2\text{M}_3\text{O}_{12}$ and $\text{ABM}_3\text{O}_{12}$ families, which can lead to reduced thermally induced stresses within bulk polycrystals.

ACKNOWLEDGMENTS

B.A.M. is grateful to CNPq (National Council for Scientific and Technological Development) for a Research Productivity Grant. L.P.P. and P.I.P. are grateful to CNPq for scholarships. The authors are grateful to undergraduate student Gabriella Faro for technical assistance. This study was supported by the NSERC Canada (grants to M.A.W.), and the Canada Foundation for Innovation, the Atlantic Innovation Fund and other partners that fund the Facilities for Materials Characterization managed by the Institute for Research in Materials at Dalhousie University. Aspects of this study were sponsored by the Department of the Army, U.S. Army Research Office.

REFERENCES

1. J.S.O. Evans, T.A. Mary, and A.W. Sleight: Negative thermal expansion in a large molybdate and tungstate family. *J. Solid State Chem.* **133**, 580 (1997).
2. C.P. Romao, K.J. Miller, C.A. Whitman, M.A. White, and B.A. Marinkovic: Negative thermal expansion (thermomictic) materials. In *Comprehensive Inorganic Chemistry II*, Vol. 4, J. Reedijk and K. Poeppelmeier, eds. (Elsevier: Oxford, 2013); p. 128–151.
3. C. Lind: Two decades of negative thermal expansion research: Where do we stand? *Materials* **5**(6), 1125 (2012).
4. J.S.O. Evans: Negative thermal expansion materials. *J. Chem. Soc., Dalton Trans.* **19**, 3317 (1999).
5. J.S.O. Evans, T.A. Mary, and A.W. Sleight: Negative thermal expansion materials. *Phys. B Condens. Matter.* **241**–**243**, 311 (1997).
6. S. Sumithra and A.M. Umarji: Negative thermal expansion in rare earth molybdates. *Solid State Sci.* **8**(12), 1453 (2006).
7. M. Ari, P.M. Jardim, B.A. Marinkovic, F. Rizzo, and F.F. Ferreira: Thermal expansion of $\text{Cr}_{2x}\text{Fe}_{2-2x}\text{Mo}_3\text{O}_{12}$, $\text{Al}_{2x}\text{Fe}_{2-2x}\text{Mo}_3\text{O}_{12}$ and $\text{Al}_{2x}\text{Cr}_{2-2x}\text{Mo}_3\text{O}_{12}$ solid solutions. *J. Solid State Chem.* **181**(6), 1472 (2008).
8. T. Varga, J.L. Moats, S.V. Ushakov, and A. Navrotsky: Thermochemistry of $\text{A}_2\text{M}_3\text{O}_{12}$ negative thermal expansion materials. *J. Mater. Res.* **22**(9), 2512 (2007).
9. A.L. Goodwin, S.A. Wells, and M.T. Dove: Cation substitution and strain screening in framework structures: The role of rigid unit modes. *Chem. Geol.* **225**(3–4), 213 (2006).
10. K.J. Miller, M.B. Johnson, M.A. White, and B.A. Marinkovic: Low-temperature investigations of the open-framework material $\text{HfMgMo}_3\text{O}_{12}$. *Solid State Commun.* **152**(18), 1748 (2012).
11. J.S.O. Evans and T.A. Mary: Structural phase transitions and negative thermal expansion in $\text{Sc}_2(\text{MoO}_4)_3$. *Int. J. Inorg. Mater.* **2**(1), 143 (2000).
12. B.A. Marinkovic, P.M. Jardim, R.R. de Avillez, and F. Rizzo: Negative thermal expansion in $\text{Y}_2\text{Mo}_3\text{O}_{12}$. *Solid State Sci.* **7**(11), 1377 (2005).
13. B.A. Marinkovic, M. Ari, R.R. de Avillez, F. Rizzo, F.F. Ferreira, K.J. Miller, M.B. Johnson, and M.A. White: Correlation between AO_6 polyhedral distortion and negative thermal expansion in orthorhombic $\text{Y}_2\text{Mo}_3\text{O}_{12}$ and related materials. *Chem. Mater.* **21**(13), 2886 (2009).
14. M.M. Wu, Y. Zu, J. Peng, R.D. Liu, Z.B. Hu, Y.T. Liu, and D.F. Chen: Controllable thermal expansion properties of $\text{In}_{2-x}\text{Cr}_x\text{Mo}_3\text{O}_{12}$. *Cryst. Res. Technol.* **47**(7), 793 (2012).
15. C.P. Romao, F.A. Perras, U. Werner-Zwanziger, J.A. Lussier, K.J. Miller, C.M. Calahoo, J.W. Zwanziger, M. Bieringer, B.A. Marinkovic, D.L. Bryce, and M.A. White: Zero thermal expansion in $\text{ZrMgMo}_3\text{O}_{12}$: NMR crystallography reveals origins of thermoelastic properties. *Chem. Mater.* **27**(7), 2633 (2015).

16. K.J. Miller, C.P. Romao, M. Bieringer, B.A. Marinkovic, L.P. Prisco, and M.A. White: Near-zero thermal expansion in $\text{In}(\text{HfMg})_{0.5}\text{Mo}_3\text{O}_{12}$. *J. Am. Ceram. Soc.* **96**(2), 561 (2012).
17. W. Song, B. Yuan, X. Liu, Z. Li, J. Wang, and E. Liang: Tuning the monoclinic-to-orthorhombic phase transition temperature of $\text{Fe}_2\text{Mo}_3\text{O}_{12}$ by substitutional co-incorporation of Zr^{4+} and Mg^{2+} . *J. Mater. Res.* **29**(7), 849 (2014).
18. A.M. Gindhart, C. Lind, and M. Green: Polymorphism in the negative thermal expansion material magnesium hafnium tungstate. *J. Mater. Res.* **23**(1), 210 (2008).
19. B.A. Marinkovic, P.M. Jardim, M. Ari, R.R. De Avillez, F. Rizzo, and F.F. Ferreira: Low positive thermal expansion in $\text{HfMgMo}_3\text{O}_{12}$. *Phys. Status Solidi* **245**(11), 2514 (2008).
20. W.B. Song, E.J. Liang, X.S. Liu, Z.Y. Li, B.H. Yuan, and J.Q. Wang: A negative thermal expansion material of $\text{ZrMgMo}_3\text{O}_{12}$. *Chin. Phys. Lett.* **30**(12), 126502 (2013).
21. W.B. Song, J.Q. Wang, Z.Y. Li, X.S. Liu, B.H. Yuan, and E.J. Liang: Phase transition and thermal expansion property of $\text{Cr}_{2-x}\text{Zr}_{0.5x}\text{Mg}_{0.5x}\text{Mo}_3\text{O}_{12}$ solid solution. *Chin. Phys. B* **23**(6), 066501 (2014).
22. F. Li, X. Liu, W. Song, B. Yuan, Y. Cheng, H. Yuan, F. Cheng, M. Chao, and E. Liang: Phase transition, crystal water and low thermal expansion behavior of $\text{Al}_{2-2x}(\text{ZrMg})_x\text{W}_3\text{O}_{12}\cdot n(\text{H}_2\text{O})$. *J. Solid State Chem.* **218**, 15 (2014).
23. T. Suzuki and A. Omote: Zero thermal expansion in $(\text{Al}_{2x}(\text{HfMg})_{1-x})(\text{WO}_4)_3$. *J. Am. Ceram. Soc.* **89**(2), 691 (2006).
24. A.W. Sleight and L.H. Brixner: A new ferroelastic transition in some $\text{A}_2(\text{MO}_4)_3$ molybdates and tungstates. *J. Solid State Chem.* **7**(2), 172 (1973).
25. B.A. Marinkovic, M. Ari, P.M. Jardim, R.R. de Avillez, F. Rizzo, and F.F. Ferreira: $\text{In}_2\text{Mo}_3\text{O}_{12}$: A low negative thermal expansion compound. *Thermochim. Acta* **499**(1–2), 48 (2010).
26. M. Pley and M.S. Wickleider: Two crystalline modifications of RuO_4 . *J. Solid State Chem.* **178**(10), 3206 (2005).
27. W. Paraguassu, M. Maczka, A.G.S. Filho, P.T.C. Freire, F.E.A. Melo, J.M. Filho, and J. Hanuza: A comparative study of negative thermal expansion materials $\text{Sc}_2(\text{MoO}_4)_3$ and $\text{Al}_2(\text{WO}_4)_3$ crystals. *Vib. Spectrosc.* **44**(1), 69 (2007).
28. M. Wojdyr: Fityk: A general-purpose peak fitting program. *J. Appl. Crystallogr.* **43**(5 Part 1), 1126 (2010).
29. V. Sivasubramanian, T.R. Ravindran, R. Nithya, and A.K. Arora: Structural phase transition in indium tungstate. *J. Appl. Phys.* **96**(1), 387 (2004).
30. A.C. Torres Dias, C. Luz Lima, W. Paraguassu, K. Pereira Da Silva, P.T.C. Freire, J. Mendes Filho, B.A. Marinkovic, K.J. Miller, M.A. White, and A.G. Souza Filho: Pressure-induced crystal-amorphous transformation in $\text{Y}_2\text{Mo}_3\text{O}_{12}$. *Vib. Spectrosc.* **68**, 251 (2013).
31. M. Maczka, W. Paraguassu, A.G. Souza Filho, P.T.C. Freire, J. Mendes Filho, F.E.A. Melo, and J. Hanuza: High-pressure Raman study of $\text{Al}_2(\text{WO}_4)_3$. *J. Solid State Chem.* **177**(6), 2002 (2004).
32. Q.J. Li, B.H. Yuan, W.B. Song, E.J. Liang, and B. Yuan: The phase transition, hygroscopicity, and thermal expansion properties of $\text{Yb}_{2-x}\text{Al}_x\text{Mo}_3\text{O}_{12}$. *Chin. Phys. B* **21**(4), 046501 (2012).
33. T.R. Ravindran, V. Sivasubramanian, and A.K. Arora: Low temperature Raman spectroscopic study of scandium molybdate. *J. Phys. Condens. Matter* **17**(2), 277 (2005).
34. W.T.A. Harrison, A.K. Cheetham, and J. Faber: The crystal structure of aluminum molybdate, $\text{Al}_2(\text{MoO}_4)_3$, determined by time-of-flight powder neutron diffraction. *J. Solid State Chem.* **76**(2), 328 (1988).
35. J.S.O. Evans, T.A. Mary, and A.W. Sleight: Negative thermal expansion in $\text{Sc}_2(\text{WO}_4)_3$. *J. Solid State Chem.* **137**(1), 148 (1998).
36. V. Srikanth, E.C. Subbarao, and G.V. Rao: Thermal expansion anisotropy, microcracking and acoustic emission of Nb_2O_5 ceramics. *Ceram. Int.* **18**(4), 251 (1992).
37. P.M. Jardim, E.S. Garcia, and B.A. Marinkovic: Young's modulus, hardness and thermal expansion of sintered $\text{Al}_2\text{W}_3\text{O}_{12}$ with different porosity fractions. *Ceram. Int.* **42**(4), 5211 (2016).
38. C.B. Carter and M.G. Norton: *Ceramic Materials* (Springer, New York, NY, 2013).

Supplementary Material

To view supplementary material for this article, please visit <http://dx.doi.org/10.1557/jmr.2016.329>.